CSIRO PUBLISHING
www.publish.csiro.au/journals/pasa *Publications of the Astronomical Society of Australia*, 2007, **24**, 1–12

The SkyMapper Telescope and The Southern Sky Survey

S. C. Keller[A,B], *B. P. Schmidt*[A], *M. S. Bessell*[A], *P. G. Conroy*[A], *P. Francis*[A], *A. Granlund*[A], *E. Kowald*[A], *A. P. Oates*[A], *T. Martin-Jones*[A], *T. Preston*[A], *P. Tisserand*[A], *A. Vaccarella*[A] *and M. F. Waterson*[A]

[A] Research School of Astronomy and Astrophysics, Australian National University, Cotter Rd, Weston ACT 2611, Australia
[B] Corresponding author. Email: stefan@mso.anu.edu.au

Received 2006 December 14, accepted 2007 February 19

Abstract: This paper presents the design and science goals for the SkyMapper telescope. SkyMapper is a 1.3-m telescope featuring a 5.7-square-degree field-of-view Cassegrain imager commissioned for the Australian National University's Research School of Astronomy and Astrophysics. It is located at Siding Spring Observatory, Coonabarabran, NSW, Australia and will see first light in late 2007.

The imager possesses 16 384 × 16 384 0.5-arcsec pixels. The primary scientific goal of the facility is to perform the Southern Sky Survey, a six-colour and multi-epoch (four-hour, one-day, one-week, one-month and one-year sampling) photometric survey of the southerly 2π sr to $g \sim 23$ mag. The survey will provide photometry to better than 3% global accuracy and astrometry to better than 50 milliarcsec. Data will be supplied to the community as part of the Virtual Observatory effort. The survey will take five years to complete.

Keywords: telescopes — surveys — techniques: photometry

1 Project Overview

SkyMapper is amongst the first of a new generation of dedicated, wide-field survey telescopes to start operation in the coming five years. It is now feasible to tessellate the field of view of a low f-number telescope with CCDs and achieve areal coverage comparable to that obtained with photographic Schmidt cameras. The all-sky photographic surveys of the Palomar and UK Schmidt telescopes (Reid et al. 1991; Holmberg et al. 1974) are currently unsurpassed in the optical. Such photographic surveys have several shortcomings however, they do not provide photometry to better than 0.2 mag, or astrometry to better than 0.5 arcsec.

Several groups are now actively pursuing digital multi-colour surveys of the sky, notably Pan-Starrs (operational 2007, Kaiser et al. 2002) and the Large Synoptic Survey Telescope (first light in 2012, Claver et al. 2004). The only survey already in progress is the Sloan Digital Sky Survey (SDSS, York et al. 2000). SDSS has mapped close to πsr of the northern sky in five colours. The gamut of scientific applications for SDSS data spans properties of the asteroid population (Ivezić et al. 2001) to the discovery of the most distant quasar (Fan et al. 2001). In the infrared, VISTA (Lewis et al. 2006) plans to survey the southern sky starting in early 2007. Other large aperture survey instruments are planned such as ESOs VST (first light 2007, Cappellaro et al. 2004) and the Lowell Observatorys Discovery Channel Telescope (first light 2009, Sebring et al. 2004) with narrower fields of view designed for targeted deeper surveys.

SkyMapper will perform the multi-colour, multi-epoch Southern Sky Survey (S3). Reflective of our science goals we have devised a filter set for the S3 that is optimised for stellar astrophysics. We have sought a filter set that best discriminates the important stellar parameters of effective temperature, surface gravity and metallicity. This is not to the detriment of non-stellar science as these areas are well served by a series of broadband filters.

The SkyMapper focal plane will feature a mosaic of 32 2048 × 4096 CCDs coupled to high speed device controllers for rapid, low noise readout. The facility will operate in an automated manner and require minimal operational support. On site there is a scheduling and data quality assurance system. Data are transferred via a high-speed link to the Australian National University's Supercomputing Facility where the data-reduction pipeline resides. SkyMapper will see first light in 2007.

2 The SkyMapper Telescope

2.1 Site

The SkyMapper telescope is located 20 m north-east of the summit of Siding Spring Mountain, near Coonabarabran, NSW (altitude 1163 m). Figure 1 shows a plan of the observatory site. To minimise the facility's impact on the seeing obtained with the telescope, large heat sources such as power supplies, computers and instrumentation within the enclosure are cooled by chilled water supplied from an equipment pad 40 m downhill from the telescope.

 10.1071/AS07001 1323-3580/07/01001

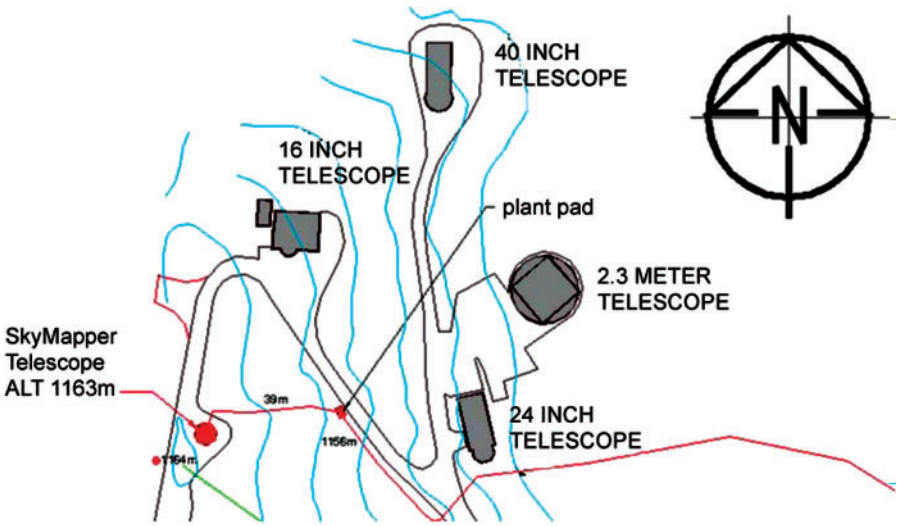

Figure 1 Plan of the SkyMapper site on Siding Spring Mountain.

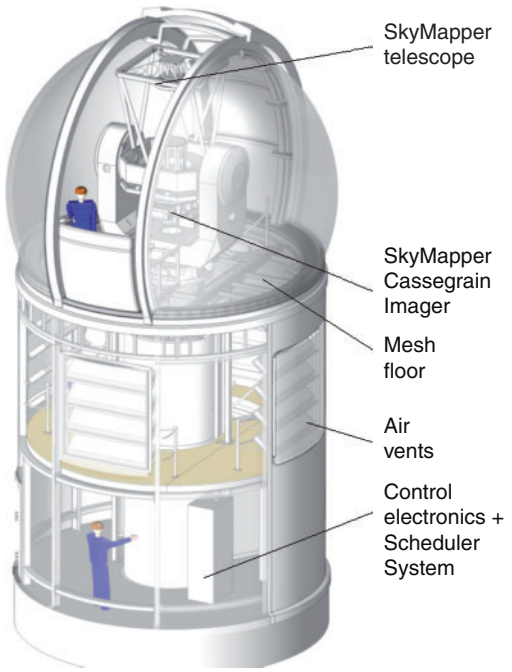

Figure 2 The SkyMapper enclosure.

2.2 *Enclosure*

The SkyMapper enclosure is 6.5 m in diameter and 11 m high with three internal levels as shown in Figure 2. The first level houses the electronics and control computers and is thermally isolated from the rest of the building. Four sets of vent shutters are set into the walls of the second level. When observing, these shutters enable passive ventilation of the observing space above via the mesh floor of the observing space. The vent shutters will have controlled opening angles to flush the observing space while not introducing excessive wind buffeting.

During the day the volume of levels two and three will be sealed and actively cooled to the expected ambient temperature at the start of observing for the night ahead. The interior of the dome will be finished matt black to minimise scattered light reaching the detector.

The SkyMapper enclosure features internal and external arrays of weather sensors. These will prevent operation in inclement weather. Should mains power fail, there will be sufficient power in the enclosure's UPS to safely shut down the facility.

Lightning is a significant risk for the facility as Siding Spring Mountain is exposed to severe summer thunderstorms (the vicinity receives approximately three strikes per km^2 per year). The mountain top is largely outcropping bedrock of high resistivity. Our lightning mitigation consists of a series of six air terminals that connect to a radial ground plane of buried copper braid that radiates 20 m from the enclosure. In addition, the telescope control computer will receive information from a commercial lightning warning service and will close the enclosure in the case of an impending thunderstorm.

2.3 *Site Conditions*

The prevailing astronomical conditions at the site are an important input to the design of the project. We have examined the weather logs of the Anglo-Australian Telescope (AAT) from 2000 to 2005 (C. McCowage, private communication). The weather patterns of Siding Spring Observatory (SSO) show little seasonal variation, with an average of 2110 hours (64%) of the time useable throughout the year, of which 1135 hours (35%) is photometric.

Using DIMM measurements (Wood, Rodgers & Russell 1995) the median free air seeing at SSO is approximately 1.1 arcsec. This assumes the turbulence is not near the ground and therefore the actual seeing may be somewhat worse. This is borne out by the logs of the AAT which are summarised in Figure 3. This shows 68% of the time the seeing is less than 1.75 arcsec.

2.4 *Optical Design*

The SkyMapper telescope optical system was designed by Electro Optics Systems, Australia. It features a 1.33-m

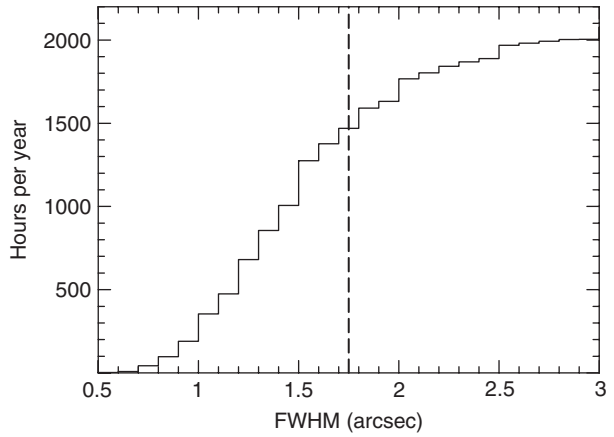

Figure 3 Seeing at Siding Spring derived from logs of the AAT.

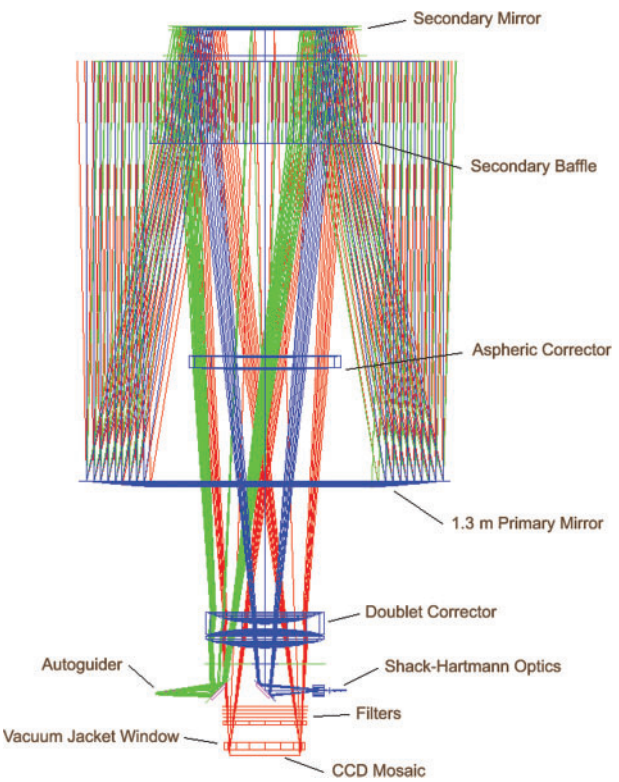

Figure 4 SkyMapper optics.

primary mirror and a relatively large 0.69-m secondary. This results in a collecting area equivalent to an unobstructed aperture of 1.13 m. The telescope is a modified Cassegrain design, optimised for wide-field operation between 340 and 1000 nm. The design is shown in Figure 4.

The primary mirror is of Astrosital glass ceramic fabricated by LZOS, Russia. The secondary mirror (sourced from SAGEM, France) is carried on an actuated hexapod system that allows for tip–tilt, x–y and telescope-focus movement. The telescope control system uses the hexapod to automatically adjust for gravity induced flexure and focus change due to temperature.

The primary and secondary mirrors possess protected aluminium coatings. This increases the longevity of the reflective surface, particularly in the UV. The three transmissive corrector elements are single-layer anti-reflection coated and composed of fused silica to maximise the UV throughput of the instrument.

Table 1. SkyMapper Imager parameters

Telescope working *f*-ratio	*f*/4.7878
Telescope focal plane scale	0.0302 mm arcsec^{-1}
Detector pixel projection	0.5 arcsec pix^{-1}
Number of pixels in mosaic	268 435 456
Mosaic dimensions	256.34 × 258.75 mm
Mosaic field of view	2.373° × 2.395°
Mosaic fill factor	91.05%
Sky coverage w. fill factor	5.68 deg^2

The EOS SkyMapper telescope is a compact, stiff and rugged structure with high mechanical natural frequencies. We expect the telescope to point to $<\pm 3$ arcsec and track to 0.5 arcsec RMS for 5 minutes in winds of <5 m s^{-1}. Both of the telescope principal axes are driven by direct on-axis DC ring motors without intervening gearboxes and direct on-axis incremental encoders. The system is therefore free of backlash.

3 The SkyMapper Imager

The SkyMapper Imager has been designed in-house at RSAA (see Granlund et al. 2006 for more details). Due to the large focal plane, the instrument is comparatively large and heavy for the size of telescope. To achieve an optimal outcome, the designs of the telescope and imager have proceeded in parallel, with close cooperation between the RSAA and Electro-Optic Systems design teams. Important imager parameters are summarised in Table 1.

Figure 5 shows the imager instrument from above looking down on the rotator interface plate. The autoguider and science filters can be seen through the beam aperture. Also seen is the Shack–Hartmann system that is used for automatic collimation and focusing. Figure 6 shows the underside of the imager. The Imager vacuum jacket is at the centre, flanked by closed-cycle helium cryocoolers and twin detector controllers. The instrument weighs ∼300 kg.

A large mechanical shutter has been fabricated by the University of Bonn, Germany. The shutter is located below the filter stack and above the vacuum jacket window. The shutter is composed of two blades that form a moving slot of variable width to provide uniform exposure of the focal plane. The shortest exposure is about 1 ms and exposure homogeneity is 0.3% in a 100-ms exposure (Reif et al. 2004).

SkyMapper has six interchangeable filters, each 309-mm square and up to 15 mm thick. Table 4 lists the specifications of the filter set for the S3. Our motivation for the choice of filters is detailed in Section 5.2. The filter set is constructed of coloured glass where possible. Coloured glass filters show better throughput homogeneity across the focal plane than can be currently achieved with multilayer interference filters. The filter glass was sourced from

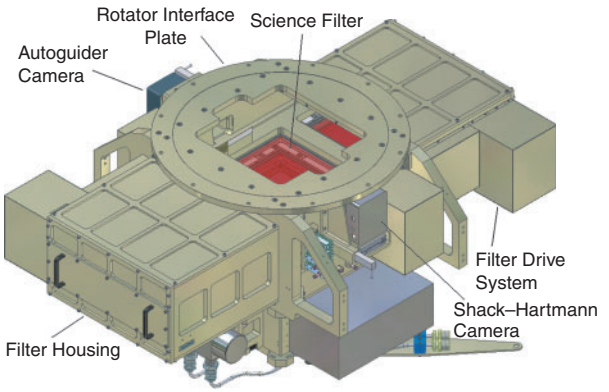

Figure 5 The SkyMapper Cassegrain Imager as seen from above.

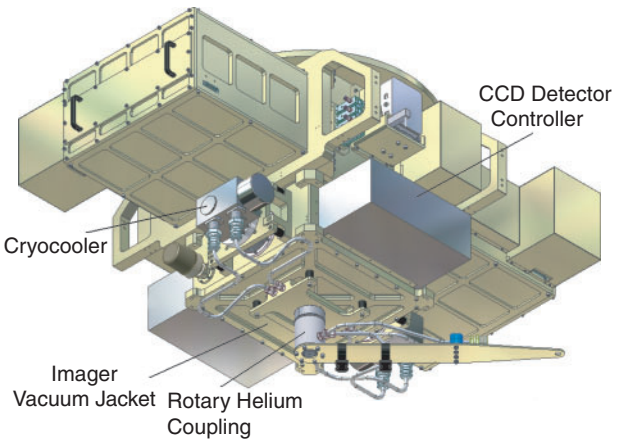

Figure 6 The SkyMapper Cassegrain Imager as seen from below.

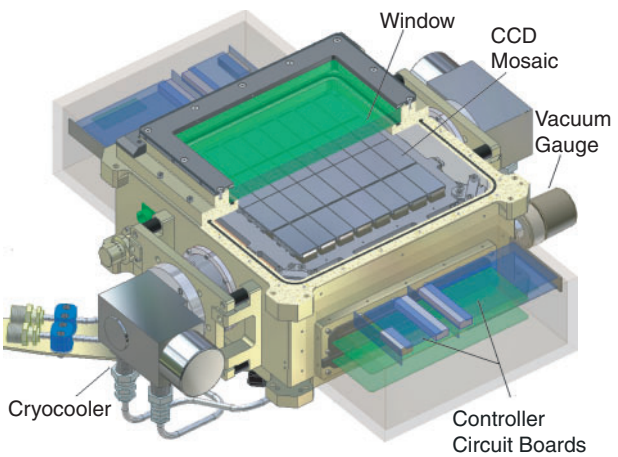

Figure 7 The SkyMapper Cassegrain Imager vacuum jacket showing the CCD mosaic.

Macro Optica, Russia, and Schott, Germany. Only the *r*- and *i*-band filters have additional short wavepass coatings to define the bandpass. An optimised anti-reflection coating will be applied to each filter by Optical Surface Technologies, USA.

The Imager vacuum jacket carries the CCD mosaic as shown in Figure 7. The vacuum jacket window is 25-mm thick fused silica with a broadband anti-reflection coating.

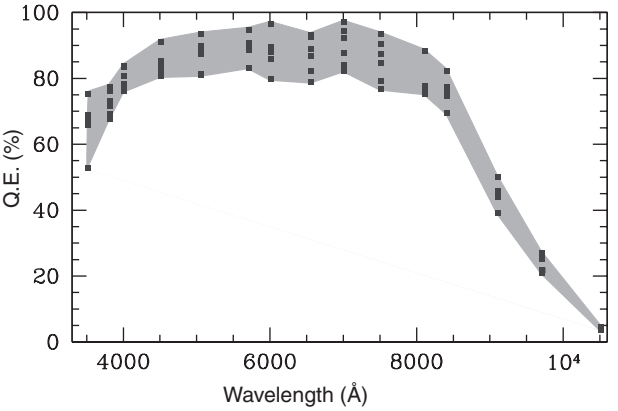

Figure 8 The spectral response of SkyMapper science CCDs. The shaded area encloses the minimum and maximum measured response for a set of six devices.

A steady flow of dry air is passed over this window to prevent condensation.

3.1 The SkyMapper Imager CCD Mosaic

The SkyMapper Imager CCD mosaic is a 4×8 array of E2V CCD44-82 detectors. Each CCD detector has 2048×4096, 15-μm^2 pixels. The deep depletion devices are back-illuminated and three-side buttable. They possess excellent quantum efficiency from 350 to 950 nm (see Figure 8), near-perfect cosmetics and low-read noise.

All 32 CCDs are carried on a 10-mm thick Invar carrier plate. The surface of the carrier plate has been machined to 10-μm flatness and on to this surface the precision pads of the E2V devices are mounted. Our aim for focal plane flatness is to match the single pixel geometric depth of field in the $f/4.78$ beam of $\pm 32\,\mu$m.

A portion of the top of the CCD detector mosaic assembly can be seen in Figure 7. The inner two rows of CCDs are butted together with a 1.5-mm gap between the rows and a 0.5-mm gap between columns. A larger gap exists between the centre and outer rows of about 4 mm. This assembly gives a filling factor of 91%.

3.2 CCD Controllers

The SkyMapper Cassegrain Imager will utilise two customised versions of the newly developed 16-channel STARGRASP controllers[1] developed for Pan-STARRS by Onaka and Tonry et al. from the University of Hawaii. A hybrid 300 MHz PowerPC CPU FPGA is used in the controller for digital signal processing. Each controller also possesses 256 MB of embedded memory for buffering the high data flows. The controllers will have integrated Gigabit Ethernet optical-fibre ports for fast readout, which will enable the SkyMapper Imager to easily meet its requirement of reading out the entire focal plane in <20 s (450 kpix s^{-1}). It is our goal to read out the focal plane in $\sim$10 s, i.e. $\sim$1 Mpix s^{-1}. This new detector controller technology will also reduce the size and weight of the controller hardware substantially and increase reliability over

[1] see http://www.stargrasp.org/

legacy systems. The controllers are to be attached to either side of the Detector Vacuum Enclosure (see Figure 7).

Both detector controllers will be connected to a single pixel server computer that transfers the data to local storage. The pixel server is commanded by the Computerised Instrument Control And Data Acquisition software system (CICADA, Young, Roberts & Sebo 1999) developed by RSAA for all observatory instruments. The RSAA's Telescope Automation and Remote Observing System (TAROS, Wilson et al. 2005) in turn controls CICADA to configure the instrument and acquire the required exposure.

4 Science Goals

The science that can be done with a comprehensive survey such as the Southern Sky Survey cannot be fully described or predicted. Data from previous all-sky surveys has been used in thousands of papers and important discoveries continue to be based upon them decades after their completion. In the following section we outline a series of scientific questions that we have identified SkyMapper will have high impact in addressing. These science goals define the requirements for SkyMapper's Southern Sky Survey.

4.1 What Is the Distribution of Solar System Objects Beyond Neptune?

The existence of quiescent comet-like objects orbiting the Sun in a region beyond Neptune was first proposed by Leonard (1930) following the discovery of Pluto. The objects in this region remained undiscovered until 1992 when the first Trans-Neptunian Object (TNO) was discovered (Jewitt & Luu 1993). Subsequent searches have, to date, uncovered more than 1000 TNOs. TNOs are believed to be debris left over from the formation of the solar system. The distributions of their orbits and masses provide important clues to the process of outer planet formation and to the origin and nature of comets. An all-sky survey will overcome the observational biases that exist in current work based around the ecliptic. Little is known about any larger TNOs, especially those on scattered orbits that take them out of the ecliptic. Models of Kenyon & Luu (1999) predict many large TNOs, some with masses larger than Pluto. The recent discovery of 2003UB313, a scattered object with a diameter slightly in excess of Pluto (Brown et al. 2006), demonstrates the possibilities for future discovery.

The requirements for this science program are as follows. By going to $r \sim 21.5$ over the entire sky we stand to discover $\sim$2000 TNOs (Trujillo et al. 2001). The motions are typically a few arcsec per hour at opposition. To distinguish nearby objects from distant ones, at least three observations are required. We envisage two epochs separated by $\sim$4 hours on the first night with a third epoch 1–3 days later. A fourth epoch after one month will be sufficient for extrapolation of the orbit to the next year. Astrometric accuracy is not particularly stringent: $<$0.2 arcsec will suffice.

4.2 What Is the History of the Youngest Stars in the Solar Neighbourhood?

In the last two decades it has been possible to definitively discern coeval, co-moving associations of young stars within the solar neighbourhood. By looking at the space motions and spatial distribution of young objects Kastner et al. (1997) revealed the TW Hya association. With the advent of all-sky X-ray and deep proper motion catalogues further close young associations were found (η Cha, Mamajek, Lawson & Feigelson 1999; Tucana-Horologium, Torres et al. 2000 and Zuckerman & Webb 2000). These associations of young stars have been recently ejected from the molecular clouds of their birth, most likely within the Sco–Cen association, a massive region of star formation in the southern Milky Way (Zuckerman & Song 2004).

Because these young stars are unobscured and close to the Sun, they are ideal targets for high-resolution imaging of protoplanetary disks with Spitzer, SOFIA and IR adaptive-optics imagers. These objects offer us a view of how stars and planetary systems form, one not obscured by the material from which they formed. While several co-moving associations have been found from the Hipparcos and Tycho catalogues, these surveys are limited to the brightest members of the cluster luminosity function.

A key requirement for this science program is to have good proper motions for objects across the sky as well as accurate colour selection down to $r = 18$. This will enable us to select nearby candidates for planetary disk searches. Relative astrometry to 50 mas over a five year baseline will provide proper motions to 4 mas year^{-1} accuracy. This is sufficient to find relevant objects to 120 pc.

4.3 What Is the Shape and Extent of the Dark-Matter Halo of Our Galaxy?

Dark matter is the dominant gravitational component of our Universe. We have few clues to its nature. One clue is its distribution. It is now clear that dark matter in the cores of galaxies does not produce central cusps of material as predicted by theory (Navarro & Steinmetz 2000). Even less is known about how dark matter is distributed in the outer regions of galaxies. For the Milky Way we would like to know the extent and shape of the dark matter: is it spherical, flattened, or triaxial? The answers to these questions place constraints on the nature of dark matter and the formation of our galaxy.

Visible dynamical tracers must be used to probe the distribution of dark matter in the galactic halo. Perhaps the best such tracers are RR Lyrae stars but such stars are rare: approximately one per 10 deg^2 beyond 50 kpc and one per 100 deg^2 beyond 100 kpc (Ivezić et al. 2001). Blue horizontal branch stars are 8–10 times more common, but require a good surface gravity discriminant to separate from the bulk of higher surface gravity main sequence stars and blue stragglers in the field. Intrinsically luminous F and G giants can be seen to greater distances but are as rare

Table 2. Southern Sky Survey defining requirements

	u	v	g	r	i	z
Sensistivity	$\sigma = 0.03$ mag $u < 20$	$\sigma = 0.03$ mag $v_s < 20$	$\sigma = 0.1$ mag $g = 21.2$	$\sigma = 0.1$ mag $r = 21.0$	3σ $i = 22.5$ detection	7σ $z = 20.5$ detection
Cadence			6 epochs hours to years	6 epochs hours to years	3 epochs for cosmic-ray rejection	3 epochs for cosmic-ray rejection
Systematic			0.03 mag			
Astrometry			50 mas over 3 years			

as RR Lyraes and similarly need a good surface gravity indicator.

Requirements for this program are a series of at least two exposures over short (∼1 week) time frame to discriminate RR Lyraes. 90% of RR Lyrae stars can be recovered with a $g - r$ colour to 0.1-mag precision and six epochs in g with a precision of 0.1 mag. Blue horizontal stars can be discriminated on the basis of colour information with a gravity indicator to distinguish contaminating blue stragglers and main-sequence A-type stars (see Section 5.2). Selection of blue horizontal branch stars and giants requires photometry accurate to ∼0.03 mag.

4.4 Extremely Metal-Poor Stars: How Did Our Galaxy Evolve?

What were the characteristics of the first stars, when did they light up the Universe, and how did they form into galaxies like the Milky Way? The formation of the first stars is a key moment in the history of the Universe yet it lies approximately 13 billion years in the past (Naoz, Noter & Barkana 2006), beyond the reach of modern-day telescopes. However, our galaxy holds a fossil record of the first generations of stars. Since the Big Bang gave rise to a universe of hydrogen, helium and an admixture of light elements, successive generations of stars have synthesized and returned to the interstellar medium the ∼4% by mass of heavier elements that comprise, for instance, the Sun. By using metallicity as a proxy for age, the most metal-poor stars are candidates for the first generation of stars. These candidates will then require follow-up spectroscopy to determine such quantities as radial velocities and fine abundance analysis.

Requisite for this program is accurate ($\sigma < 0.03$ mag) multi-colour photometry from the near-UV to the red for stars between 12 and 18 mag. Large sky coverage is essential as such stars are extremely rare. The choice of filters should provide optimal determination of effective temperature, surface gravity and metallicity.

4.5 High-Redshift QSOs: When Did the First Stars in the Universe Form?

We know that within 1.5 billion years after the Big Bang, some galaxies had formed; this is evidenced by galaxies observed to $z \sim 6$. Even at this epoch most of the intergalactic medium was ionized as evidenced by the lack of continuum absorption redward of Lyman α (the Gunn–Peterson effect, Gunn & Peterson 1965). It must be concluded that some objects must have existed earlier that produced sufficient UV flux to ionise nearly all the baryonic matter in the Universe.

The SDSS located a series of $z > 5.8$ quasars including the most distant object at $z = 6.42$ (Fan et al. 2001). The most distant QSO does seem to show continuous Lyman α absorption (Becker et al. 2001). This is our first glimpse of the interface between the ionised intergalactic medium we see locally and the neutral material before. The description of this surface tells us about the physics of the era of reionisation (Wyithe & Loeb 2004).

So far three high-redshift objects from the SDSS show the Gunn–Peterson effect. By covering the entire southern sky we stand to take this to a dozen or more such objects. Requirements for this program are survey sensitivities matching those of SDSS. Multiple epochs are essential for good cosmic ray rejection.

The union of the above requirements provides the defining (most difficult to achieve) constraints of the survey. They are summarised in Table 2.

4.6 Non-Survey Science

Planetary transits: SkyMapper allows monitoring of a large field of view to high stability (relative flux to better than 0.01 mag) making it a highly competitive facility for this purpose.

Supernovae: We are proposing to use time that does not meet the survey's seeing and sky background constraints to undertake a supernova (SN) survey. Such a survey will provide continuous coverage of 1250 deg^2 of sky, and discover approximately 100 SN Ia to $z < 0.085$ per year. In addition to allowing a systematic exploration of the statistical properties of type Ia SN, it will also serve to populate the SN Ia Hubble Diagram in this low-redshift regime. Similarly, for core-collapse SN we will increase statistics with which to explore the energetics and nucleosynthetic production of these explosions. The SN survey will lead to the detection of many hypernovae with which to explore the relationship between these objects and Gamma-Ray Bursts.

Table 3. SkyMapper main survey depth in *AB* magnitudes[A]

	u	*v*	*g*	*r*	*i*	*z*
1 epoch	21.5	21.3	21.9	21.6	21.0	20.6
6 epochs	22.9	22.7	22.9	22.6	22.0	21.5

[A]Signal-to-noise of 5, 110-second exposures.

Table 4. SkyMapper filter pass bands

Filter	50% Cut-on edge (Å)	50% Cut-off edge (Å)	FWHM (Å)
u	3250	3680	430
v	3670	3980	310
g	4170	5630	1460
r	5550	7030	1480
i	7030	8430	1400
z	8520	9690[A]	1170[A]

[A]*z* filter is unblocked at red end, the red edge is limited by the CCD sensitivity cut off in the near-IR.

5 Southern Sky Survey Design

The requirements of Table 2 are met by the design of the Southern Sky Survey that we now detail. Our science goals emphasize the need for wide sky coverage. We have defined 4069 fields covering the 2π sr of the southern sky.

5.1 Survey Coverage and Cadence

To meet our science goals we must capture variability on short and long timescales. Since most variable astronomical objects have timescales for variability ranging from hours (RR Lyraes, asteroids), months (supernova, long period variables) and years (QSOs, stellar parallax and proper motions) our survey design will ensure that each field is observed in each filter on six epochs with approximately the following cadence, $t = 0$, $+4$ hours, $+1$ day, $+1$ week, $+1$ month and $+1$ year.

The six epochs will be spatially offset slightly from each other according to a dither pattern. This will ensure that chip gaps and defects do not occult the same area of sky. At completion, 90% of the sky will be covered at least five times and 100% imaged three or more times.

The survey is to be completed in five years to realize its full potential. Together with the weather constraints detailed in Section 2.3, we have defined our exposures to be 110 seconds (plus a 20-second overhead between exposures) in each filter. Two data releases are planned: a first data release when three epochs in each filter have been obtained and calibrated and a second when the complete set of six epochs in each filter have been obtained. The expected survey depths in 1.5-arcsec seeing for a 5σ detection in *AB* magnitudes are given in Table 3.

5.2 Optimised for Stellar Astrophysics: Filter Set Design

The filter set we have designed for S3 provides both interoperability with existing systems such as SDSS and key information for the science goals discussed in Section 4. The specification of the filter set is given in Table 4. In Figure 9 we show the expected throughput of the SkyMapper Telescope and Cassegrain Imager. We have taken as our basis the Gunn & Thuan *griz* filter set (Thuan & Gunn 1976) utilized by SDSS[2]. When compared to the SDSS system the SkyMapper system features twice the throughput in *u* and three times the throughput in *z*, albeit with our smaller aperture. The cleanly separated *i* and *z* filters are optimal for discovery of high-redshift QSOs (Lyman α in *z* equates to a redshift of greater than 5.8). Photometric redshifts for $z < 0.5$ galaxies are facilitated by broadband photometry over the optical spectrum.

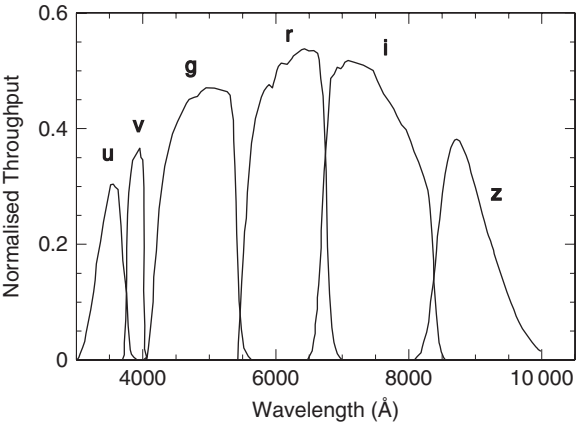

Figure 9 The expected throughput ex-atmosphere of the filter set for the Southern Sky Survey.

A large part of the science potential of SkyMapper is bound to the study of stellar populations. It was important, therefore, for us to consider how we can best characterize stellar populations using broad to intermediate band photometry. To do this we computed the synthetic colours of stars spanning metallicity, surface gravity, effective temperature and extinction from Pietrinferni et al. (2006) model atmospheres. For any given point in the colour–colour space, the number of synthetic models within an error ellipsoid provides the measure of uncertainty in the derived quantities. These simulations were performed as a function of photometric uncertainty and filter choice.

For G stars and hotter the main discriminating power is derived from the near-UV. We incorporate a Strömgren *u* filter and an intermediate band filter similar to DDO38, we term *v*, that covers the spectrum from 3670 to 3980 Å. These two filters are able to break the degeneracy between surface gravity and metallicity as illustrated by the following important applications.

5.2.1 Application 1: Blue Horizontal Branch Stars

In Figure 10 we consider the uncertainty in the derived stellar surface gravity, *g*, as a function of temperature for stars of $\log g = 2.5$ and 4.5 with photometric uncertainties of 0.03 mag per filter. For hot O and B stars the intensity

[2] http://www.astro.princeton.edu/PBOOK/camera/camera.htm

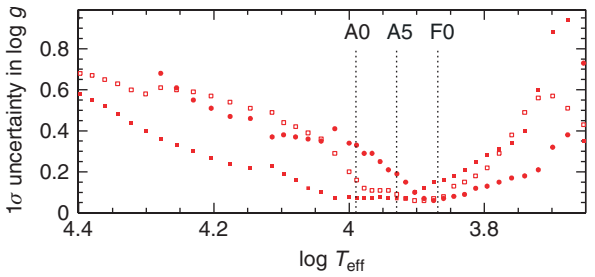

Figure 10 The 1σ uncertainty in surface gravity derived under photometric uncertainties of 0.03 mag from the SkyMapper filter set. Solid squares are $\log g = 4.5$, open squares $\log g = 3.5$ and circles $\log g = 2.0$. Dashed vertical lines show the temperatures corresponding to spectral types on the main sequence.

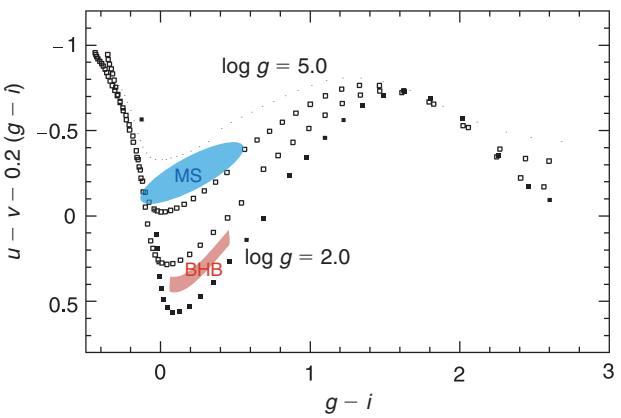

Figure 11 $u - v$ vs. $g - i$ for stars of solar metallicity and a range of surface gravity. Blue horizontal branch stars are well separated from main-sequence and blue straggler stars.

of the Balmer-jump feature is not significantly affected by changes in surface gravity. Consequently we have limited ability to discern surface gravity for such stars. Similarly, for stars cooler that 5000 K (G6–7V) the Balmer jump disappears as a spectral feature. However, for A-type stars we expect to determine the surface gravity to ∼10%. This range in temperature is inhabited by blue horizontal branch stars (BHBs), standard candles for the Halo.

A sightline through the halo inevitably contains local disk main-sequence stars and blue stragglers in the temperature range of interest. However, these contaminants are of significantly higher surface gravities than those of BHBs. The u and v filters measure the Balmer jump and the effect of H opacity which increases with surface gravity. As can been seen from Figure 11, the $u - v$ colour index discriminates between BHBs and their contaminants. The separation is 0.5 mag in colour. On the basis of our photometric selection we will be able to discern a sample of BHBs to a distance of 130 kpc with less than 5% contamination.

5.2.2 *Application 2: Extremely Metal-Poor Stars*

Amongst cooler stars, the u and v filters capture the magnitude of metal line blanketing, a general suppression of the continuum blueward of ∼4000 Å. In Figure 12 we show the uncertainty in derived metallicity as a function

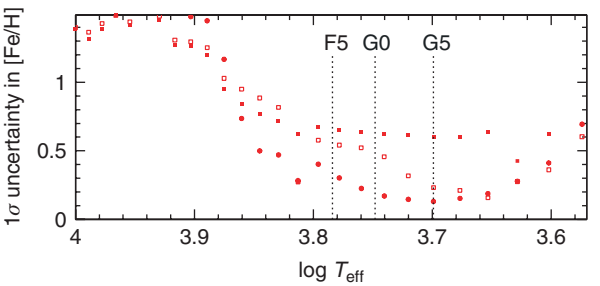

Figure 12 The 1σ uncertainty in metallicity derived under photometric uncertainties of 0.03 mag from the SkyMapper filter set. Solid squares represent [Fe/H] = −4 models, open squares [Fe/H] = −2 and circles [Fe/H] = 0.

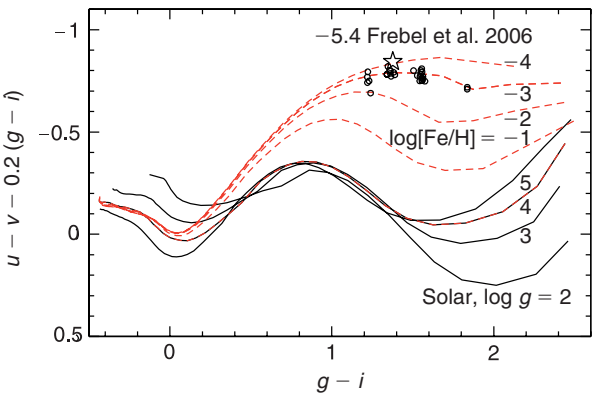

Figure 13 $v - g$ vs. $g - i$ for stars of solar metallicity and a range of surface gravity (solid lines) and for $\log g = 4$ and metallicities to [Fe/H] = −4. Overlaid are the computed colours of HE1327–2326 (Frebel et al. 2005) and the sample of extremely metal-poor stars from Cayrel et al. (2004).

of temperature for stars of metallicity [Fe/H] = −4 from the S3 filter set.

We are able to determine [Fe/H] best at high metallicity and the uncertainty rises to ±0.7 dex at [Fe/H] = −4. At extremely low metallicities the density of stars drops by a factor of ten for every factor of ten drop in metallicity. Consequently, the challenge in finding extremely metal-poor stars (EMPs) is to keep the very small subset of interesting objects clean from photometric outliers. In this regard, the S3 filter set provides improved separation over existing filter sets between the bulk of halo stars of [Fe/H] > −2 and those of [Fe/H] < −4. This provides us a distinct advantage in isolating extremely metal-poor stars from photometric colours.

Our ability to discern metallicity is not clearly expressed in a colour–colour plot as the vector of grad metallicity is not closely aligned with any colour. The best correspondence between grad metallicity and our colours is found with the $v - g$ colour shown in Figure 13. We see that $v - g$ has little dependence on surface gravity from early F to mid G, however this breaks down as we enter the cooler K-type range. The evolved extremely metal-poor stars do not possess temperatures as cool as K0 and those cooler than K0 and still on the main-sequence are

sufficiently lacking in luminosity to make their numbers small over the survey volume.

We have calculated the number of halo stars in the survey brighter than $g = 18.1$ (where we reach a signal-to-noise ratio of 33 in the first data release) by integrating the Bahcall and Soniera galactic model (Bahcall & Soneira 1980) over the survey area with galactic latitude greater than 15°. We then scale by the results of the Hamburg ESO Survey (Christlieb 2003) to find the number of stars with [Fe/H] < -4. There are on order of a thousand such stars, including a hundred of metallicities less than -5. Follow-up will be tractable; to recover 90% of the stars of [Fe/H] > -4 will require intermediate resolution spectroscopy of $\sim$2600 stars. High signal-to-noise 8-m spectra will be required on the distilled sample of extremely metal-poor stars for detailed elemental abundance studies.

6 Photometric Calibration

To calibrate the S3 to the required global accuracy of 0.03 mag we will perform a shallow survey of the entire southern sky under photometric conditions (the Five-Second Survey). Exposure times of approximately five seconds in each filter will enable us to obtain photometry for stars from 8.5 to 15.5 mag. The Five-Second Survey will consist of a set of at least three images of each field in all filters. The network of standards will provide the photometric and astrometric catalogue to which the deeper Main Survey images will be anchored. With all-sky coverage, the Five-Second Survey will enable the Main Survey images (and any other images taken with the telescope) obtained in non-photometric conditions to be calibrated.

The major impediment to the derivation of accurate photometry from wide field of view instruments is the influence of scattered light. Magnier & Cuillandre (2004) studied the systematic errors in the flat-field structure of the CFHT12K imager. By dithering a standard star sequence over the CCDs of the mosaic they were able to form a map of the photometric residuals (observed minus expected) over the focal plane (a photometric superflat). In the case of the CFHT12K imager systematic errors in the flatfield amount to 5% peak-to-peak: around half due to pixel scale change across the camera, another half due to the effect of scattered light. The scattered-light component arises from ambient light scattered off surfaces within the enclosure and telescope reaching the detector. We have sought to minimise the scattered light by finishing the interior surfaces matt black, however some scattered light will inevitably remain.

Forming a photometric superflat is a direct way to remove the signature of scattered light. During commissioning, we will establish a series of six calibration fields at declination $\sim -25°$ (to avoid the zenith keyhole of the telescope) around the sky. By observing the calibration fields with a series of dithers and rotator angles we will be able to characterise and correct for departures from photometric flatness as a function of position on the detector array. These fields will also serve as our secondary standard star fields. During Five-Second Survey operations we will acquire standard star fields every 90 minutes. At such time the two highest fields will be observed, thus providing a range of airmasses from $\sim$1 to 1.8.

With full coverage of right ascension a photometric 'ring closure solution' can be formed (see for example Pel & Lub 2006). The ring closure solution ensures that the differential flux ratios between calibration fields in all bandpasses are very accurately determined. This, finally, leaves the zeropoints of the flux in each filter to be determined. We will define the absolute zero point of the SkyMapper system from the Walraven photometric system (Pel & Lub 2006) and the associated stars in the Next Generation Spectral Library[3]. To do this we will first use the Walraven photometry to accurately zeropoint the spectrophotometric standards. We will then use the spectrophotometric standards and with our photometric bandpasses, to derive absolute zeropoints. Initially our photometric bandpasses will be those measured by a laboratory monochromometer convolved with the CCD spectral response and adjusted to match the observations of standard stars. Ultimately, we plan to use a monochromatic flat + NIS standard (Stubbs et al. 2006) to characterise the response of our system.

7 Astrometric Calibration

Our astrometric calibration uses as its basis the UCAC2 astrometric catalogue (Zacharias et al. 2004). The calibration has two stages. Firstly, UCAC2 stars in common to Five-Second images are used to define an image world coordinate system (WCS). The UCAC2 provides between 40 and several hundred stars per SkyMapper CCD. Our derived positional uncertainties are better than 50 mas for bright stars. The Main Survey images are then astrometrically calibrated against the stars of the Five-Second Survey.

We implement the ZPN[4] coordinate representation. This representation utilizes a radial term to characterise distortions across the image and a simple linear transformation to remove the effects of rotation, scale, and any shear caused by refraction. Since most distortion is radial from the optical axis, the ZPN system is able to linearise a distorted optical plane with a single term. Linearising the telescope system in this way provides robust coordinate transformations across the images with no difficulties in CCD corners or in images with few astrometric standards.

Any systematic astrometric offsets will be applied via a lookup table after processing a large portion of the survey. These are not expected, but would be difficult to accurately quantify if they depend on the rotator angle of the telescope. Differential atmospheric refraction will be corrected for once the colours of each object are determined. Over five years and 36 epochs, it will be possible to derive proper motions to ± 4 mas year^{-1}.

[3] http://lifshitz.ucdavis.edu/mgregg/gregg/ngsl/ngsl.html
[4] Zenithal/azimuthal polynomial projection see Calabretta et al. (2004).

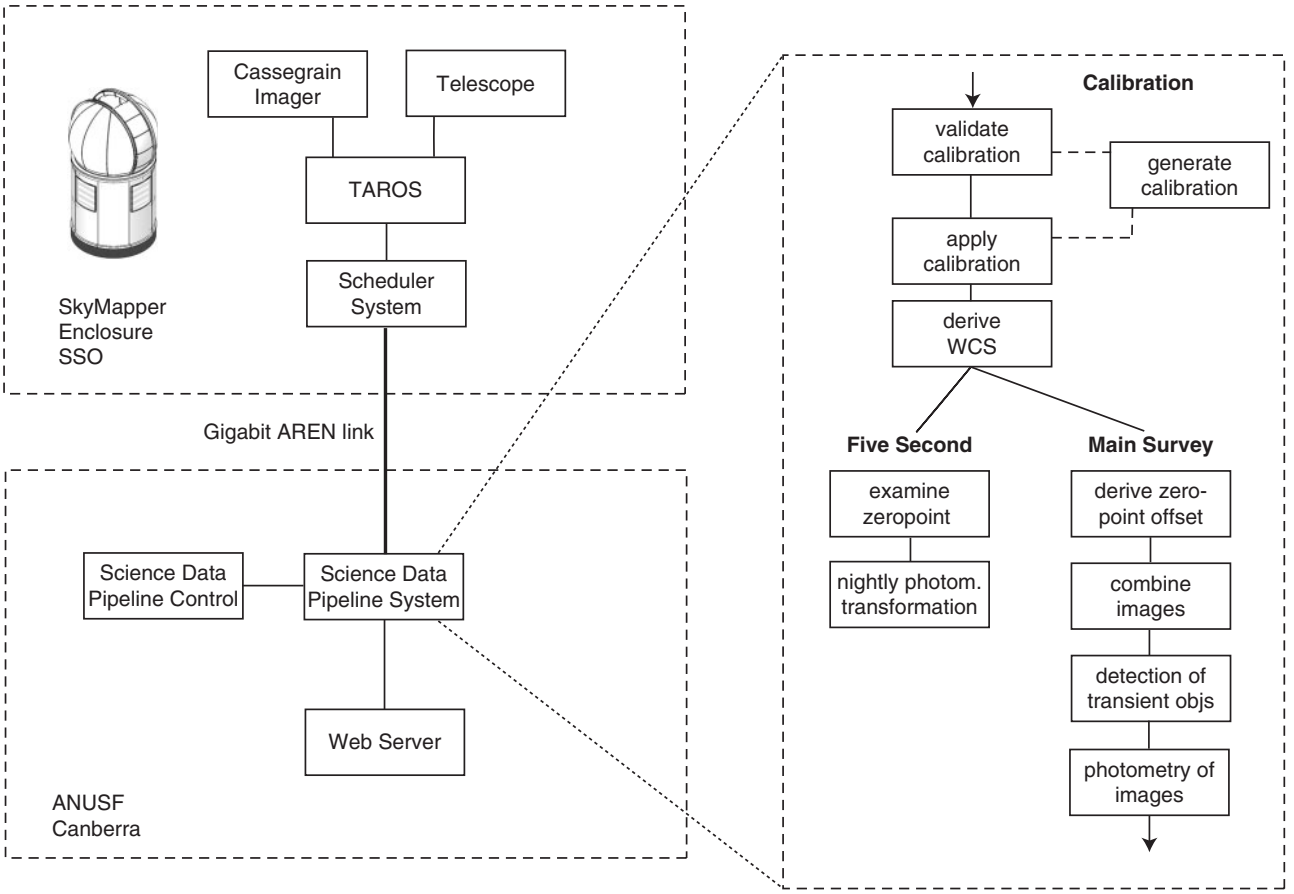

Figure 14 A system level view of the SkyMapper Scheduler and Science Data Pipeline.

8 SkyMapper Data Acquisition & Reduction

The acquisition and reduction of SkyMapper data are managed by the Scheduler and Science Data Pipeline Systems respectively. A schematic system level diagram is given in Figure 14. We now discuss the two systems in detail.

8.1 The Scheduler System

The on-site Scheduler System is responsible for scheduling the required calibration and science data. In the course of a typical night, first bias frames will be acquired then sky flatfields for as many filters as time permits. As each exposure is completed, the data are checked for quality and system changes. In the case of the bias frames we check that the bias levels are nominal. This is a simple check of the health of the detector system. Before astronomical twilight a focusing sequence will be performed. Alternatively, when available, the Shack–Hartmann system will be used to determine the telescope focus.

At the end of evening astronomical twilight, SkyMapper will begin the task of acquiring S3 images. The required instrument configuration is supplied by the Scheduler System to the instrumentation via the TAROS interface. At detector readout the next instrument configuration is issued by the Scheduler System to the telescope in order to minimise latency. The CCD devices are read out to a 5-TB RAID array and the local disk. The copy of the image on local disk is used for data quality checks so as not to impede the writing of data to the RAID array.

The Five-Second Survey holds top priority in scheduling as this data must be obtained under photometric conditions. A manually set flag tells the Scheduler System if the night is likely to be photometric based on predicted weather conditions from the Australian Bureau of Meteorology MLAPS model. If this flag is set, the scheduler will commence taking any required (and possible) Five-Second Survey data. After writing the acquired data to disk the Scheduler System performs a check of the photometric zeropoint and the surface brightness in one CCD image. Rapidly fluctuating zeropoints or zeropoints below a nominal value indicate the presence of cloud.

Should the conditions become non-photometric during the night the Scheduler System will switch to the Main Survey. The Main Survey can continue under uniform diminished transparency such as might occur with light cirrus. If the transparency drops below a threshold then the data are flagged of poor quality and the field is made available for rescheduling. Due to time constraints for quality checks we do not attempt to monitor the uniformity of transparency across all 32 CCDs of a field within the Scheduler System. This check is performed in the Science Data Pipeline described below.

Another critical aspect of image quality, the seeing, is also monitored by the Scheduler System. The Main Survey

will have a seeing limit of ∼1.75 arcsec (the 68th percentile of seeing). The remainder of the time will be given to a poor seeing program. In the case of the Five-Second Survey, an upper limit of 2.5 arcsec will suffice before the poor seeing program is pursued.

Data are trickled throughout the night and proceeding morning to the ANU Supercomputing Facility (ANUSF) via a gigabit link. A winter night of Five-Second Survey data (a maximal constraint) can be transferred over several hours. At completion of observing the dome will close and the telescope will park. The enclosure air conditioning will aim for the next night's expected temperature as predicted by the MLAPS model.

8.2 The Science Data Pipeline System

Data reduction is managed by the Science Data Pipeline System (SDPS) running at the ANUSF, Canberra. The SDPS has been designed specifically for S3 data. Figure 14 outlines the stages of the SDPS for data from the Five-Second and Main Surveys. The system consists of a series of modules that perform the required calibration, photometric standardisation, catalogue generation, photometry, and data delivery via the Internet.

Pipeline modules are implemented in C/C++ for numerically intensive processes, with PERL scripting to facilitate process flow. Pipeline progress is tracked, and results recorded, in a POSTGRESQL database. Individual modules are queued for execution on the Australian Partnership for Advanced Computing SGI Altix 3700Bx2 cluster housed at ANUSF.

The SDPS stages are as follows. Firstly, for each completed night we check the nightly median bias against the median bias generated from the bias frames obtained on many (up to 30) nights preceding the night in question. If the nightly median bias is outside nominal bounds the system attempts to generate a new median bias to apply. A similar sanity check is applied to the flatfields obtained. If a comparison of the nightly flatfields with the current authorized flatfield is outside bounds, such as might occur due to a change in the optical system of the telescope caused by, for example, the deposition of dust, the system will attempt to generate a new median flatfield to apply to this and subsequent nights' data. When flatfield change occurs, there may not be sufficient numbers of flatfields to be combined to form an authorized flatfield and several nights' worth of data may not be able to be processed until such time as sufficient flatfields are obtained and an authorized flatfield produced.

In addition to the bias and flatfield calibration files, fringe frames are generated for i and z. Skyflats are generated from the median of science images in each band. Skyflats are produced to remove most of the effects of scattered light in the system. We then derive a photometric superflat for each filter to characterize the residual effects of scattered light. The photometric superflat is formed by imaging of our calibration fields (Section 6). We form a median image from the residuals between our reference photometry and that obtained from images after bias, flat, fringe and skyflat application. It is necessary to regenerate the fringe, skyflat and superflat whenever the flatfield changes as all are intimately related to the optical path. For quality control, the processes that generate calibration data require the astronomer to authorize the new calibration files before they are applied to any data.

A world coordinate system is defined for each CCD image as described in Section 7. Once the Five-Second Survey data are in place, we test uniformity of transparency across each Main Survey image by deriving the zeropoints of all CCDs and examining their deviations from nominal. Significant spatial variation of zeropoints indicates the presence of non-uniform cloud attenuation. Such an image is rejected from further processing.

At this stage the image is ready for extraction of photometry and astrometry. The SDPS has two streams for the two data types, the Five-Second and Main Surveys.

For each night of five-second data the zeropoints of all images are considered. Excessive variation indicates the night was not photometric and the data are discarded. Aperture photometry is performed on the images. We then derive the nightly transformation equations from the photometry derived from the calibration fields that are interleaved with our five-second observations. We then apply the transformation equations to the data residing in the five-second database.

Main Survey images are reduced when three (first data release) or six (second data release) images of a field have been obtained in all six filters and corresponding five-second data exists. Firstly, the zeropoint offset between each image and the corresponding Five-Second survey photometry is found on a chip by chip basis. The photometry for each image is then corrected for this offset to draw the potentially non-photometric Main Survey data onto the standard instrumental magnitude system.

We combine the set of images in each filter. In doing so, we mask saturated stars and grow their associated bleeding, remove satellite trails and remove cosmic ray tracks. Objects within the combined image are detected to 7σ. Transient objects will not be retained in the median frame. In order to capture transients we mask the objects found from the median image in each component image and then look for detections greater than 10σ. A final catalog is constructed as the union of all detections in the g, r, i, and z bands, as well as any transient objects.

Photometry is performed upon the complete catalog of objects. For each object, flux will be measured via PSF-fitting, aperture (over a range of apertures), Petrosian, and Kron photometry[5]. In addition, photometry will also be forced to occur in fixed position mode (useful at low SNR), and where the centroid of the object is allowed to drift. Classification of object type will occur utilising Source Extractor's neural network. Galaxy photometry is obtained in two modes: firstly, using the galaxy shape as determined from the image with the most signal and,

[5] Using modified Source Extractor code, Bertin & Arnouts (1996).

secondly, using the shape parameters from each median filter image. The resulting object positions, photometry and shape parameters are stored in the S3 database.

The Five-Second Survey represents 75 TB worth of data, the Main Survey another 150 TB. This data are retained, in raw and reduced forms, at the ANUSF's Mass Data Store, a robotic tape archive of PB size. It is estimated that the database of photometry for the Main Survey will amount to of order 5 TB.

9 Data Products

The first SkyMapper data product will be the Five-Second Survey database. This will be released when a ring closure solution has been established for the calibration fields (see Section 6). These photometric data will be accessible from the survey website. The website will offer the ability to perform simple relational queries on the database of photometry.

We envisage two Main Survey data releases for each field; one when three epochs in all filters have been obtained and a second when the final set of six observations have been obtained. The data release will staged after adequate quality control has been undertaken. In addition to database queries of the Main Survey photometry, external users will have access to the reduced, combined images.

Acknowledgments

SkyMapper is funded by the Australian National University and supported by grants from the Australian Research Council. Weather information from the AAT logs was kindly provided by Chris McCowage and Steven Lee of the AAO.

References

Bahcall, J. N. & Soneira, R. M., 1980, ApJS, 44, 73
Becker, R. H., et al., 2001, AJ, 122, 2850
Bertin, E. & Arnouts, S., 1996, A&AS, 117, 393
Brown, M. E., Schaller, E. L., Roe, H. G., Rabinowitz, D. L. & Trujillo, C. A., 2006, ApJ, 643, L61
Calabretta, M. R., Valdes, F., Greisen, E. W. & Allen, S. L., 2004, ASPC 314, ADASS XIII, Eds. Ochsenbein, F., Allen, M. G. & Egret, D. (San Francisco: Astronomical Society of the Pacific), 551
Cappellaro, E., Capaccioli, M., Mancini, D., Sedmak, G., Baruffolo, A., Cascone, E. & Greggio, L., 2004, BaltA, 13, 683
Cayrel, R., et al., 2004, A&A, 416, 1117
Christlieb, N., 2003, RvMA, 16, 191
Claver, C. F., et al., 2004, SPIE, 5489, 705
Fan, X., et al., 2001, AJ, 122, 2833
Frebel, A., et al., 2005, Natur, 434, 871
Granlund, A., Conroy, P. G., Keller, S. C., Oates, A. P., Schmidt, B., Waterson, M. F., Kowald, E. & Dawson, M. I., 2006, SPIE, 6269, 69
Gunn, J. E. & Peterson, B. A., 1965, ApJ, 142, 1633
Holmberg, E. B., Lauberts, A., Schuster, H. E. & West, R. M., 1974, A&AS, 18, 463
Ivezić, Ž., et al., 2001, AJ, 122, 2749
Jewitt, D. & Luu, J., 1993, Natur, 362, 730
Kaiser, N., et al., 2002, SPIE, 4836, 154
Kastner, J. H., Zuckerman, B., Weintraub, D. A. & Forveille, T., 1997, Sci, 277, 67
Kenyon, S. J. & Luu, J. X., 1999, AJ, 118, 1101
Leonard, F. C., 1930, ASPL, 1, 121
Lewis, J. R., Irwin, M. J., Gonzalez-Solares, E. A., Bunclark, P. S., Hodgkin, S. T., Evans, D. W. & McMahon, R. G., 2006, ASPC 351, ADASS XV, Eds. Gabriel, C., Arviset, C., Ponz, D. & Solano, E. (San Francisco: Astronomical Society of the Pacific), 255
Magnier, E. A. & Cuillandre, J.-C., 2004, PASP, 116, 449
Mamajek, E. E., Lawson, W. A. & Feigelson, E. D., 1999, PASA, 16, 257
Naoz, S., Noter, S. & Barkana, R., 2006, MNRAS, 373, 98
Navarro, J. F. & Steinmetz, M., 2000, ApJ, 528, 607
Pel, J. W. & Lub, J., 2006, in The Future of Photometric, Spectrophotometric and Polarmetric Standardisation, Ed. Sterken, C., Blankenberge, Belgium, ASP Conf. Series.
Pietrinferni, A., Cassisi, S., Salaris, M. & Castelli, F., 2006, ApJ, 642, 797
Reid, I. N., et al., 1991, PASP, 103, 661
Reif, K., Klink, G., Müller, P. & Poschmann, H., 2004, Scientific Detectors for Astronomy, The Beginning of a New Era, Eds. Amico, P., Beletic, J. W. & Beletic, J. E. (Kluwer), 367
Sebring, T. A., Dunham, E. W. & Millis, R. L., 2004, SPIE, 5489, 658
Stubbs, C. W., et al., 2006, preprint (astro-ph/0609260)
Thuan, T. X. & Gunn, J. E., 1976, PASP, 88, 543
Torres, C. A. O., da Silva, L., Quast, G. R., de la Reza, R. & Jilinski, E., 2000, AJ, 120, 1410
Trujillo, C. A., Jewitt, D. C. & Luu, J. X., 2001, AJ, 122, 457
Wilson, G., et al., 2005, ASPC 347, ADASS XIV, Eds. Shopbell, P., Britton, M. & Ebert, R. (San Francisco: Astronomical Society of the Pacific), 563
Wood, P. R., Rodgers, A. W. & Russell, K. S., 1995, PASA, 12, 97
Wyithe, J. S. B. & Loeb, A., 2004, Natur, 427, 815
York, D. G., et al., 2000, AJ, 120, 1579
Young, P. J., Roberts, W. H. & Sebo, K. M., 1999, ASPC 172, ADASS VIII, Eds. Mehringer, D. M., Plante, R. L. & Roberts, D. A. (San Francisco: Astronomical Society of the Pacific), 115
Zacharias, N., Urban, S. E., Zacharias, M. I., Wycoff, G. L., Hall, D. M., Monet, D. G. & Rafferty, T. J., 2004, AJ, 127, 3043
Zuckerman, B. & Webb, R. A., 2000, ApJ, 535, 959
Zuckerman, B. & Song, I., 2004, ARA&A, 42, 685